

# The exact convex roof for GHZ-W mixtures for three qubits and beyond

Andreas Osterloh<sup>1</sup>

<sup>1</sup>Quantum Research Center, Technology Innovation Institute, Abu Dhabi, P.O. Box 9639, UAE  
(Dated: July 2024)

I present an exact solution for the convex roof of the square root threetangle for all states within the Bloch sphere. The working hypothesis is that optimal decompositions contain as many states from the zero-polytope as possible which can be called zero-state locking. The footprint of the measure of entanglement consists in a characteristic pattern for the fixed pure states on the surface which form the optimal solution. The solution is subject to transformation properties due to the SL-invariance of the entanglement measure.

## I. INTRODUCTION

Although we know that entanglement is everywhere present where there is interaction, it is difficult to measure it, because the operator one has to measure is non-Hermitian and consequently the eigenvalues are complex values for every pure states. We therefore take its absolute value to quantify this important resource, which is indispensable for quantum computing[1–4], quantum communication[5–8], and quantum sensing in general[9–16]; quantum technology is working because these non-local quantum correlations are there. Reasonably, as a non-local quantity, entanglement has to be invariant under the change of the local basis and permutations of the local entities. This leads to the concept of LOCC invariance and the monotone property[17] that every good entanglement measure must satisfy. In general one has to prove this monotone property, which is granted for, when extending the local invariance group from  $SU(n)$  to  $SL(n)$ [18] for  $n$  being the number of different axis of the local entity one can do rotations about. In general, the quantities obtained through this extension have the elegant property of being merely susceptible for entanglement at a global level, discarding everything which is non-global. Thus, they are measures of genuine multipartite SL-entanglement[19, 20]. Examples for taking qubits as local entities are the concurrence[21, 22] and the threetangle[23].

The monotone property has included already the convex-roof extension to arbitrary mixed states. However, the calculation of it turns out to be a difficult task, which even is thought to be NP-hard[24, 25] (see however [26]). For very few examples we have an exact solution for evaluating this convex-roof, as for the concurrence for two qubits. These are examples for which the pure state measure scales linear in  $\rho$ ; it generally holds if the corresponding  $d$ -th root of a tangle of degree  $2d$  is connected to a bilinear functional as does the concurrence. This happens for the threetangle but only for certain states[27]. This is not so in general, and the zero-polytope consists of four independent solutions. However, for the mixture of GHZ and W states and the square root of the threetangle it is known[28–30] that the Bloch-sphere has two tetrahedra in it: one is the zero-polytope and the other is the polytope made of three of the states of the zero-

polytope and the GHZ state.

Based on the conjectured property of zero-state locking[27, 31], in a recent work[27] it has been established how optimal decompositions will behave for rank-2 density matrices (see Fig. 1). Optimal decompositions are limited to at most 4 states[32, 33], i.e. to three dimensional simplices for this case. We use the nomenclature

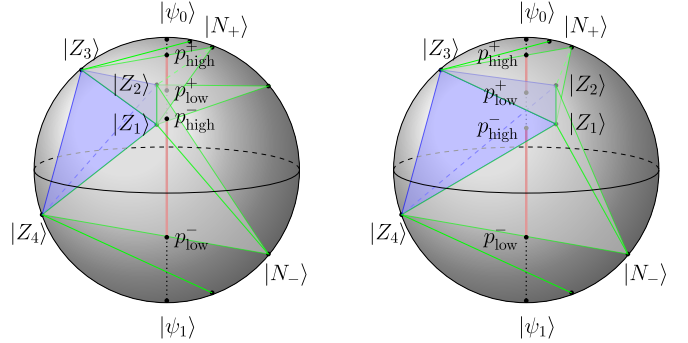


FIG. 1. Polytopes of type  $3^+N$  (left figure) and  $3^+S$  (right figure), taken from Ref. [27]. To the zero polytope (blue) entangled polytopes (gray) are added with corresponding pure states  $|N_{\pm}\rangle$ . It was noted that a pure state will be added for every of the faces of the zero polytope, which are four in this particular case. For symmetry requirements  $|N_{\pm}\rangle$ , as well as the pure states of the  $(2, 1)$  decompositions, are situated in  $\phi = 0$ . This condition will be relaxed with the symmetry here, because of the non-intersection property of optimal decompositions. The optimal decompositions, here indicated by green lines, brachiate through this structure of polytopes with the additional pure state at  $\phi = 0$ .

$(n_z, n_e)$  of this work for identifying the decompositions, where  $n_z$  is the number of states from the zero polytope, and  $n_e$  that of entangled pure states in the decomposition. In particular, it has been observed that for each three surface elements of the zero polytope there is precisely one entangled pure state  $|N\rangle$  forming a  $(3, 1)$  polytope. Within polytopes the entanglement varies linearly due to convexification. These pure states  $|N_i\rangle$  need to be found as a convexification point of  $(1, 1)$  and  $(2, 1)$  decompositions. Optimal decompositions do not intersect, and this fills out good part of the Bloch-sphere. Then, for the tips of each two connected surface elements,  $|N_{i1}\rangle$  and  $|N_{i2}\rangle$ , out of the pure entangled states  $|N_i\rangle$

found before, are connected by a line of pure entangled states. These give further  $(2,1)$  decompositions in the Bloch sphere. All remaining decompositions will be of the type  $(1,1)$ . This excludes the possibility of optimal  $(0, n_e)$  decompositions for  $n_e > 1$ ; there are strong arguments for this to hold[27], but no general proof exists. Optimality of  $(n_z, n_e)$  have been excluded numerically through case studies[27]. The transformation property, also of optimal decomposition states[30, 34], is an important finding and lifts the results of this work to all states being SL-equivalent to the mixed state in consideration.

This work is laid out as follows. At first we will deduce those pure states  $|N_i\rangle$  which form optimal  $(3,1)$  decompositions, then find the lines interconnecting each pair of the entangled pure states  $|N_i\rangle$ . The remaining space of the Bloch-sphere is filled with  $(1,1)$  decompositions.

*The pure entangled states  $|N_i\rangle$*  – We analyze the Bloch sphere of the rank-two mixed state

$$\rho[p] = p|GHZ\rangle\langle GHZ| + (1-p)|W\rangle\langle W| \quad (1)$$

where  $|GHZ\rangle = (|111\rangle + |000\rangle)/\sqrt{2}$  and  $|W\rangle = (|100\rangle + |010\rangle + |001\rangle)/\sqrt{3}$ . A three-fold rotational symmetry due to cyclic permutations of the qubits exist for both states. Therefore, it is enough to perform the classification in a wedge of the Bloch sphere given by the azimuthal angle  $\phi \in [-\pi/3, \pi/3]$  only. The rest of the sphere is obtained by symmetry requirements.

One of the pure entangled state is the maximally entangled GHZ state[28, 30]. This is also confirmed through the convexification procedure of  $(2,1)$  and  $(1,1)$  decompositions which correctly points to the GHZ state. Remains to find the state in one of the three vertical wedges of the Bloch sphere. One possibility is to choose another orthogonal basis for the same Bloch sphere. The one orthogonal decomposition chosen here is the real one of the three pure states of the zero-polytope together with its orthogonal partner. These are given by

$$|Z_3\rangle = \sqrt{p_0}|GHZ\rangle - \sqrt{1-p_0}|W\rangle \quad (2)$$

$$|Z_{3,\perp}\rangle = \sqrt{1-p_0}|GHZ\rangle + \sqrt{p_0}|W\rangle \quad (3)$$

with  $p_0 = \frac{4\sqrt[3]{2}}{3+4\sqrt[3]{2}}$  [28]. The relevant characteristic curves for  $(1,1)$  decompositions with the W state and  $(2,1)$  decompositions with  $(|Z_1\rangle + |Z_2\rangle)/\sqrt{2}$  are shown in Fig. 2 together with their convexification. It shows that at  $p_c = 0.0964142$  the line is a proper convexification, starting from zero and touching the curve for  $(2,1)$  decompositions; the  $(1,1)$  decompositions are shown in blue. The corresponding pure state is located in  $p_2(p_1, \phi_1, p_c) = 0.00673174$ . Since  $p_c < 1/2$ , this corresponds to an angle  $\theta_1 = \pi - \arccos(2p_c - 1) = 0.164279 = 9.4125^\circ$ , which adds up to the angle of  $|Z_{3,\perp}\rangle$ , which is  $\theta_0 = 1.8273 = 104.697^\circ$ . The angle of the new state is hence calculated to be  $\theta = \theta_0 + \theta_1 = 1.99158 = 114.109^\circ$ . The four tetrahedra are shown in grey in Fig. 7 with green edges. This is confirmed from the convexification procedure with the  $(1,1)$  decompositions (with  $|W\rangle$  here)

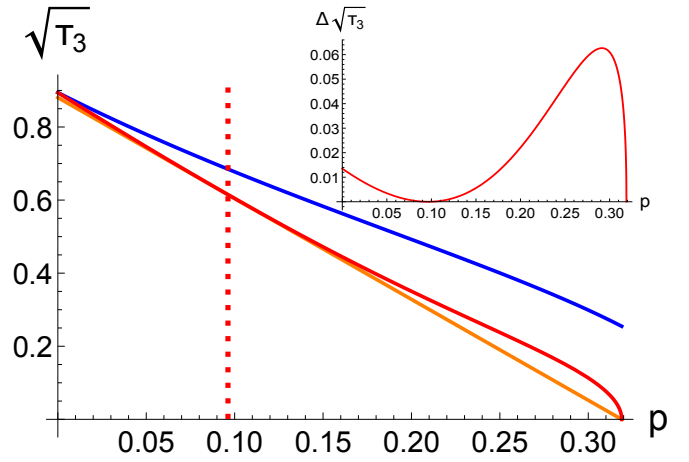


FIG. 2. Convexification procedure of  $|Z_3\rangle$  mixed with the corresponding orthogonal state. The curves are made convex with a line touching at  $p_c = 0.0964142$ , as is highlighted in the inset, where we plot the difference in  $\sqrt{T_3}$  of the  $(1,1)$  decompositions with  $|Z_3\rangle$  and the convex line. The  $(2,1)$  decompositions with  $|Z_3\rangle$  and  $|W\rangle$  are shown in blue above both curves.

for eigenstates being situated at an angle  $\theta = 140^\circ$ . Invoking the three-fold symmetry for this case leads to the three optimal  $(3,1)$  decompositions with the states  $|N_i\rangle$ ,  $i = 1, 2, 3$ , as a tip. This shows as well that in this case  $(2,1)$  decompositions are optimal in the direction of  $|GHZ\rangle$  and  $(1,1)$  decompositions are optimal in the direction of  $|W\rangle$ . Fig 7 shows these  $(2,1)$  decompositions as blue lines on the Bloch sphere surface. In [27], much

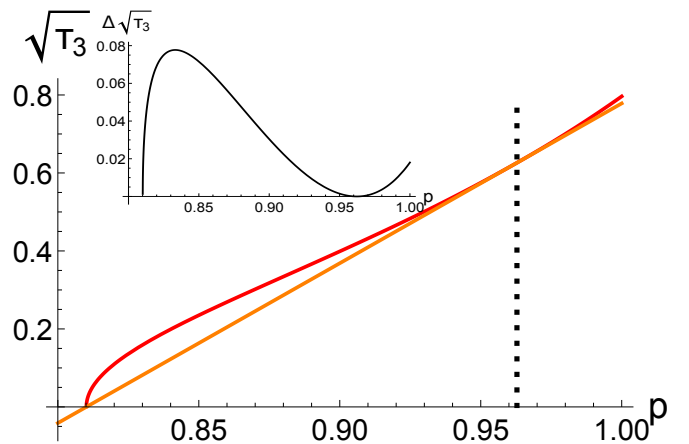


FIG. 3. Convexification procedure of the two corresponding pure states lying on the line given by the vector  $|Z_1\rangle + |Z_2\rangle$  in a mixed state. The curves are made convex with a line touching at  $p_c = 0.962243$ , as is highlighted in the inset, where we plot the difference in  $\sqrt{T_3}$  of the  $(1,1)$  decompositions with  $|Z_3\rangle$  and the convex line. The  $(2,1)$  decompositions with  $|Z_3\rangle$  and  $|W\rangle$  are above both curves; they are not shown here.

effort has been given concerning the distribution of optimal decompositions. These findings hold for even more general SL-invariant tangles  $\tau$  than the threetangle, de-

ected by  $\sqrt{\tau_3}$ , and the observations here agree with it. We emphasize that the simplices of  $|GHZ\rangle - |Z_1\rangle - |Z_2\rangle$  is co-planar with  $|Z_1\rangle - |Z_2\rangle - |N_1\rangle$ ; so are the simplices  $|Z_1\rangle - |N_1\rangle - |W\rangle$  and  $|Z_1\rangle - |N_3\rangle - |W\rangle$ .

*Optimal (2,1) decompositions in between the states  $|N_i\rangle$*  – In order to get a glimpse of what is happening in between the lower tetrahedra, we briefly want to see the case in which a density matrix lies within this simplex of (2,1) decompositions. For symmetry reasons, this is the case for the two pure states lying respectively on the vectors corresponding to  $|Z_1\rangle + |Z_2\rangle$  or to  $|Z_3\rangle + |W\rangle$ . The two cases lead to the same result, and we will describe explicitly the first case of  $|Z_1\rangle + |Z_2\rangle$ . The corresponding characteristic curves can be viewed in Fig. 3. It is seen that a convexification leads here to a  $p_c = 0.962243$  which corresponds to  $p_2(p_0, \pi, p_c) = 0.989858$  for the corresponding pure state on the Bloch sphere surface. This leads to an angle  $\theta_1 = 0.201758 = 11.5599^\circ$ . As before we have to consider that the two eigenstates lie at an angle  $\theta_0 = 2.0539 = 117.68^\circ$ . So, the angle of the state  $|M_3\rangle$  is  $\theta = \theta_0 + \theta_1 = 2.25566 = 129.24^\circ$ . The three points corresponding to the states  $|M_i\rangle$  for  $i = 1, 2, 3$  are marked in Fig. 7 with white dots.

For the further points in the Bloch sphere, we rely on a direct comparison of (2,1) with (1,1) decompositions. We therefore chose the connecting line between  $|N_3\rangle$  and  $|M_3\rangle$ ; the complete solution is obtained by applying the three-fold symmetry. It is important noticing that, at first sight, the effective tangle of (2,1) and (1,1) decompositions yield the same result. That this is not so is seen by looking at the difference between (1,1) and (2,1) decompositions, shown in Fig. 4.  $\lambda$  refers to the parameter convexly connecting  $|N_3\rangle$  and  $|M_3\rangle$ , whereas  $\lambda_2$  is the corresponding parameter for  $|W\rangle$  and  $|Z_3\rangle$ . It is seen that

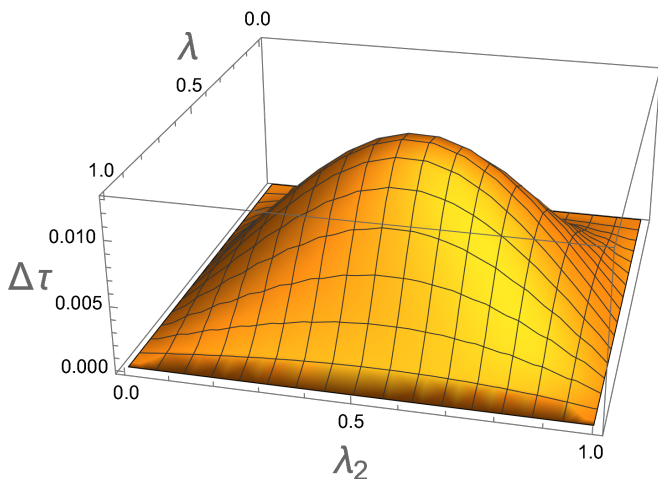


FIG. 4. Difference of  $\sqrt{\tau_3}$  of (1,1) and (2,1) decompositions of  $|W\rangle$  and  $|Z_3\rangle$  for states connecting  $|N_3\rangle$  and  $|M_3\rangle$ .

the states under consideration get optimised by choosing the (2,1) decomposition. We optimize the tangle with respect to  $\lambda_2$ . The pure states are located in the posi-

tions indicated in Fig. 5. This leads to the lower blue

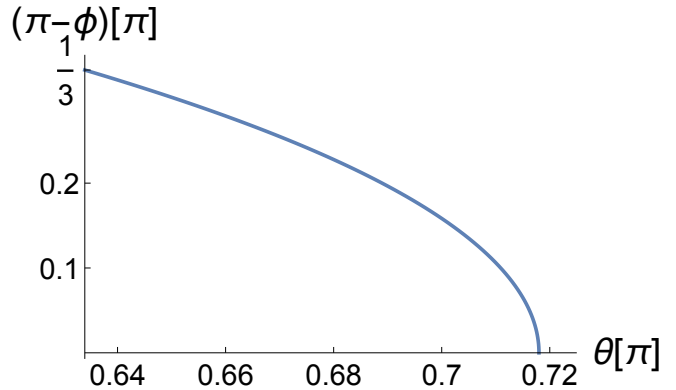


FIG. 5. Positions of the entangled pure state in the (2,1) decompositions of  $|W\rangle$  and  $|Z_3\rangle$  for states connecting  $|N_3\rangle$  and  $|M_3\rangle$ .

curves shown in Fig. 7 which lie on a circle that is not a grand circle as the ones before; instead it has a distance to the center of the Bloch sphere of 0.0711148. There are numerical errors to this, but they are small and only occur in the border regions, where the difference to the (1,1) decompositions tends to vanish (see Fig. 6) That

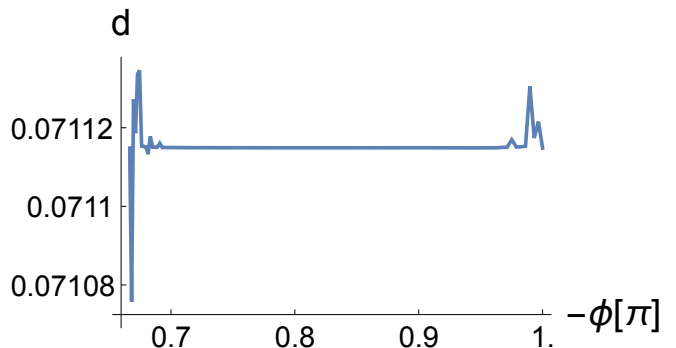


FIG. 6. Difference of  $\sqrt{\tau_3}$  of (1,1) and (2,1) decompositions of  $|W\rangle$  and  $|Z_3\rangle$  for states connecting  $|N_3\rangle$  and  $|M_3\rangle$ .

the states form a circle is confirmed by calculating the derivative with respect to the angle and showing its orthogonality to the original vector (not shown here). The numerical error scales with  $\Delta\phi^2$  as expected. The normal direction of the circle is  $(0.57589, 0, -0.81753)$ . Using the symmetry, we get the three points of normal vectors together with a dashed line in blue. The same is done for the azimuthal grand circles.

For the remaining points in the Bloch sphere there is only a single visible state from the zero polytope left which leads to (1,1) decomposition being optimal there. They are depicted in Fig. 7 by green lines and red points.

*Conclusions* – The mixture of GHZ and W state has been elaborated for all the Bloch sphere, obtaining a pattern on the surface that is characteristic for these two states in the mixture. The finding is based on the zero-

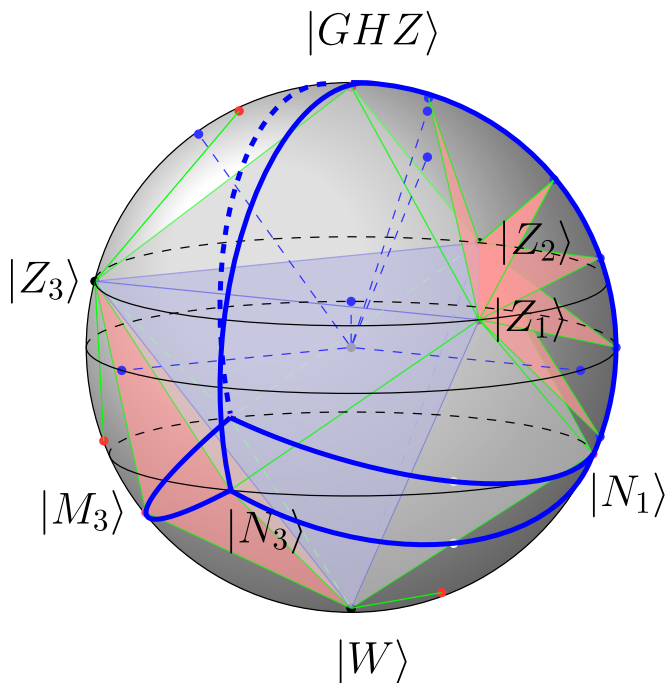


FIG. 7. Optimal decompositions are obtained for the rank-two mixtures of GHZ and W state and are depicted here graphically. It consists of the zero polytope (blue shaded), 4 polytopes defined by three of the zero states together with a state  $|N\rangle$  one of which is the GHZ state itself (grey shaded); all these polytopes are three dimensional. On top of this kernel structure of five polytopes are three lines along grand circles along  $\phi$  direction and three lines which are on circles with a distance 0.0711148 to the center of the Bloch sphere. Along these lines move pure states which form a two-dimensional optimal decomposition (red triangles). Blue points mark the position of the respective normal vectors on the Bloch sphere surface; blue lines the corresponding pure states in  $(2,1)$  decompositions. All remaining parts of the Bloch sphere are covered by  $(1,1)$  decompositions.

state locking and that  $(n_z, n_e)$  decompositions for  $n_e > 1$  are not optimal for the present case. We have checked this numerically but there is no general proof for that finding. For the zero-state locking it is essential to look at a certain roots of the tangle, which is the square root in the case of the thretriangle. The Bloch sphere is divided into the zero polytope and four polytopes onto each faces of the zero polytope with corresponding four pure states. The faces of two neighboring such polytopes are strictly planar. There are pure states that belong to  $(2,1)$  decompositions moving on three azimuthal grand circles and three circles which possess a small distance 0.0711148 to the Bloch sphere center. Their normal vector is  $(0.57589 \cos \phi_i, 0, -0.81753 \sin \phi_i)$ , with  $\phi_i = i2\pi/3$ . The remaining decompositions to fill the Bloch sphere are of the type  $(1,1)$ . This distribution of the optimal decomposition is natural and inter-connects the polytopes of various dimensions. For SL invariant tangles there is a transformation rule that applies in par-

ticular to the optimal decomposition states[30]. Applying these rules yields the solution for the convex-roof for these cases. For the general case the characteristic features of the convex roof will modify, but the structure will stay the same, as reported also in ref. [27]. It would be interesting to what extent the findings are universal. The paths of the pure entangled state of  $(2,1)$  decompositions here moves on circles, but this does not need to be this way. Future investigation, clarifying this question, will be needed. The analysis is based on two essential pillars: the zero-state locking and that every optimal decomposition would be of the type  $(n_z, 1)$ . It would be crucial to either prove or disprove these conjectures in future work.

This presumably clarifies how optimal decompositions of rank two mixtures behave. It will be very intriguing to understand their behavior for higher ranks.

*Acknowledgements* – I acknowledge the TII and Luigi Amico for supporting this research.

#### Appendix A: General properties of optimal decompositions for real states of rank two

For the number  $n_{\text{opt}}$  of pure states contained in any optimal decomposition holds  $\text{rank}[\rho] \leq n_{\text{opt}} \leq (\text{rank}[\rho])^2$  [32, 33]. Thus, it is sufficient to look for up to 4 such pure states that generically form three-dimensional simplices. We want to emphasize that more than the maximal 4 states may be in an optimal decomposition; in this case, since every sub-partition of an optimal decomposition is itself optimal, each 4 states out of that decomposition are optimal as well and the optimal decomposition is given by the convex polytope made out of these points. The tangle will behave linearly in these optimal polytopes. Since the states are composed of real elements every tangle  $\tau$  has the property that  $\tau(z) \equiv \tau(z^*)$  where  $|\psi\rangle \propto |\psi_1\rangle + z|\psi_2\rangle$  is a representation that corresponds to a vector onto the Bloch-sphere with the parametrization[31]

$$z \hat{=} \vec{n} = \begin{pmatrix} x \\ y \\ z \end{pmatrix} = \begin{pmatrix} 2\sqrt{p(1-p)} \cos \phi \\ 2\sqrt{p(1-p)} \sin \phi \\ 2p - 1 \end{pmatrix} \quad (\text{A1})$$

where  $|GHZ\rangle$  and  $|W\rangle$  are the two anti-podes on the  $z$ -axis. Real superpositions lie in the  $x$ - $z$ -plane.

We will be mainly interest in a) where the line  $\vec{n}_0 \vec{n}_1$  cuts the  $z$ -axis, b) which are the weights of the corresponding entangled state(s), and c) where it crosses the Bloch sphere, that is the corresponding pure states. Whereas the answer to a) is given by the probability

$$P = \frac{p_0 \sqrt{p_1(1-p_1)} \cos \phi_1 + p_1 \sqrt{p_0(1-p_0)} \cos \phi_0}{p_0 \sqrt{p_0(1-p_0)} \cos \phi_0 + p_1 \sqrt{p_1(1-p_1)} \cos \phi_1} \quad (\text{A2})$$

such that the point is located in  $\vec{n}_P = (2P - 1)\vec{e}_z$ , the

answer to b) is given by

$$\lambda = \frac{\mu_1}{\mu_0} = \frac{\sqrt{p_0(1-p_0)} \cos \phi_0}{\sqrt{p_1(1-p_1)} \cos \phi_1} \quad (\text{A3})$$

and for the mainly interesting case of  $\phi_1 = 0$  and  $p$  being the probability in the density matrix in consideration, we obtain as a solution to c)

$$P_{\pm} = p_0 + \frac{p - p_0}{2} \frac{(p - p_0)(1 - 2p_0) + 2p_0(1 - p_0) \cos^2 \phi_0 \pm \sqrt{(p_0 - p)^2 + 4pp_0(1 - p_0)(1 - p) \cos^2 \phi_0}}{(p - p_0)^2 + p_0(1 - p_0) \cos^2 \phi_0} \quad (\text{A4})$$

The resulting tangle is a convex combination of the tangle values of the respective pure states. This strictly linear

to a dimensionality of at most three.

### 1. (1,1)-decompositions

Here, we collect the formulae obtained for (1,1)-decompositions of a pure state at z-coordinate  $2p_1 - 1$ , where  $p_1$  corresponds to its probability of the two states  $|\psi_i\rangle$ ;  $i \in \{N, S\}$ . This corresponds to two pure states in the Fig. 8. We find

$$l_1(p_1, p) = 2\sqrt{(p - p_1)^2 + p_1(p_1 - 1)} \quad (\text{A5})$$

$$l_2(p_1, p) = \frac{4p(1 - p)}{l_1(p_1, p)} \quad (\text{A6})$$

$$m_2(p_1, p) = \frac{l_1(p_1, p)}{l_1(p_1, p) + l_2(p_1, p)} \quad (\text{A7})$$

$$p_2(p_1, p) = \frac{4p^2(1 - p_1)}{l_1(p_1, p)^2} \quad (\text{A8})$$

$$= (1 - p_1) \frac{p}{1 - p} \cdot \frac{l_2(p_1, p)}{l_1(p_1, p)} \quad (\text{A9})$$

$$p(p_1, p_2) = p_1 + \frac{(p_2 - p_1)\sqrt{p_1(1 - p_1)}}{\sqrt{p_1(1 - p_1)} + \sqrt{p_2(1 - p_2)}} \quad (\text{A10})$$

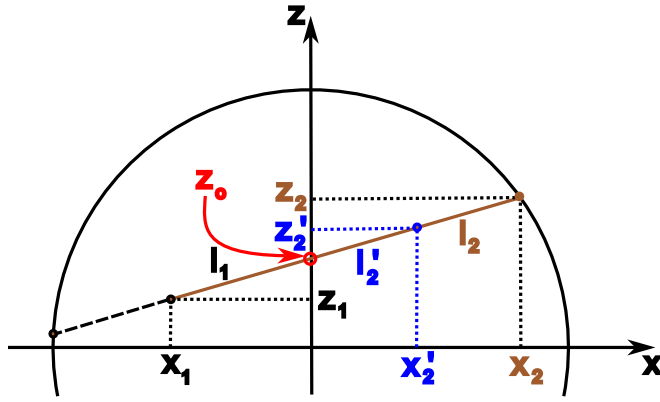


FIG. 8. States within the Bloch sphere. For a given line  $\overline{x_1 x_2}$  all triangles  $z_0 x_1 z_1$ ,  $z_0 x_2 z_2$ , and  $z_0 x'_2 z'_2$ , are similar. Ratios of their length are determined by the theorem of intersecting lines.

behavior inside all the simplices of an optimal decomposition indirectly tells about whether there needs to be one or more states in a decomposition for being optimal: the continuation of the respective decomposition type has to lead to a convex behavior in the tangle value; where this condition is not satisfied a (linear) convexification is needed. This holds in particular if the corresponding optimal polytope changes dimension. Here, this means

Next we want to examine whether for a given (1,1) decomposition with  $p_1$ ,  $p_2$ , and  $p$  it is convenient to split the pure state into two, having a (1,2) decomposition. It can be seen that the ratios  $x_1/(2|p_1 - p|) = x_2/(2|p_2 - p|) = x'_2/(2|p'_2 - p|)$  are equal with  $y'_2 = \pm\sqrt{4p'_2(1 - p'_2) - x'^2_2}$  (see Fig. 8). For the new  $p'_2$  of this new state at phase  $\phi_2$  the calculation gives

$$p'_2(p_1, p; \phi_2) = p_1 + (p - p_1) \frac{2p_1(1 - p_1) - (p - p_1)(2p_1 - 1) \cos^2 \phi_2 + \cos \phi_2 \sqrt{4p(1 - p)p_1(1 - p_1) + (p - p_1)^2 \cos^2 \phi_2}}{2(p_1(1 - p_1) + (p - p_1)^2 \cos^2 \phi_2)} \quad (\text{A11})$$

### 2. (2,2)-decompositions

In the following we will assume that two complex conjugated pairs, corresponding to a superposition of two

states at  $p_i$  and angles  $\pm\phi_i$ ,  $i \in \{1, 2\}$ , such that both

states come to lie inside the Bloch sphere projection. We find

$$m_2(p_1, \phi_1; p_2, \phi_2) = \frac{\sqrt{p_1(1-p_1)\cos^2(\phi_1)}}{\sqrt{p_1(1-p_1)\cos^2(\phi_1)} + \sqrt{p_2(1-p_2)\cos^2(\phi_2)}} \quad (\text{A12})$$

$$= \frac{l_1(p_1, \phi_1; p_2, \phi_2; p)}{l_1(p_1, \phi_1; p_2, \phi_2; p) + l_2(p_1, \phi_1; p_2, \phi_2; p)} \quad (\text{A13})$$

$$m_1(p_1, \phi_1; p_2, \phi_2) = 1 - m_2(p_1, \phi_1; p_2, \phi_2) \quad (\text{A14})$$

$$p(p_1, \phi_1; p_2, \phi_2) = p_1 + (p_2 - p_1) \frac{\sqrt{p_1(1-p_1)\cos^2(\phi_1)}}{\sqrt{p_1(1-p_1)\cos^2(\phi_1)} + \sqrt{p_2(1-p_2)\cos^2(\phi_2)}} \quad (\text{A15})$$

$$= \frac{p_2 \sqrt{p_1(1-p_1)\cos^2(\phi_1)} + p_1 \sqrt{p_2(1-p_2)\cos^2(\phi_2)}}{\sqrt{p_1(1-p_1)\cos^2(\phi_1)} + \sqrt{p_2(1-p_2)\cos^2(\phi_2)}} \quad (\text{A16})$$

$$= p_1 m_1(p_1, \phi_1; p_2, \phi_2) + p_2 m_2(p_1, \phi_1; p_2, \phi_2) \quad (\text{A17})$$

$$l_1(p_1, \phi_1; p_2, \phi_2; p) = 2\sqrt{(p_1 - p)^2 + p_1(1-p_1)\cos^2\phi_1} \quad (\text{A18})$$

$$l_2(p_1, \phi_1; p_2, \phi_2; p) = 2\sqrt{(p_2 - p)^2 + p_2(1-p_2)\cos^2\phi_2} \quad (\text{A19})$$

From this it is seen that the weights of the states are symmetric under exchanging  $p_i \rightarrow 1 - p_i$  separately for

$i \in \{1, 2\}$ . Setting  $\phi_2 = 0$ , we are in (2, 1) decompositions and the result is

$$p_2(p_1, \phi_1; p) = p_1 + (p - p_1) \frac{(p_1 - p)(2p_1 - 1) + 2p_1(1 - p_1)\cos^2\phi_1 + \sqrt{(p_1 - p)^2 + 4p(1 - p)p_1(1 - p_1)\cos^2\phi_1}}{2((p_1 - p)^2 + p_1(1 - p_1)\cos^2\phi_1)} \quad (\text{A20})$$

Next, for the evaluation of (2, 2) from (2, 1) decompositions for given  $p_1, \phi_1$ , and  $p$  the ratios of the following quantities are kept fixed (see Fig. 8):  $x_1/(2|p_1 - p|) = x_2/(2|p_2 - p|) = x'_2/(2|p'_2 - p|)$  with  $y'_2 =$

$\pm\sqrt{4p'_2(1 - p'_2) - x'^2_2}$ . These have to be substituted in  $m_2(p_1, \phi_1; p'_2, \phi'_2)$  where  $x'_2 = 2\sqrt{p'_2(1 - p'_2)}\cos\phi'_2$ .

- 
- [1] T. D. Ladd, F. Jelezko, R. Laflamme, Y. Nakamura, C. Monroe, and J. L. O'Brien, *Nature* **464**, 45 (2010).
- [2] S. S. Gill, A. Kumar, H. Singh, M. Singh, K. Kaur, M. Usman, and R. Buyya, *Software: Practice and Experience* **52**, 66 (2022).
- [3] R. Orús, S. Mugel, and E. Lizaso, *Rev. Phys.* **4**, 100028 (2019).
- [4] M. Ringbauer, M. Meth, L. Postler, R. Stricker, R. Blatt, P. Schindler, and T. Monz, *Nature Physics* **18**, 1053 (2022).
- [5] N. Gisin and R. Thew, *Nature photonics* **1**, 165 (2007).
- [6] W. Luo, L. Cao, Y. Shi, L. Wan, H. Zhang, S. Li, G. Chen, Y. Li, S. Li, Y. Wang, *et al.*, *Light: Science & Applications* **12**, 175 (2023).
- [7] D. Cazzolino, B. Da Lio, D. Bacco, and L. K. Oxenløwe, *Adv. Quant. Tech.* **2**, 1900038 (2019).
- [8] G. De Santis, K. Kravtsov, S. Amairi-Pyka, and J. A. Grieve, arXiv preprint arXiv:2406.08562 (2024).
- [9] F. A. Narducci, A. T. Black, and J. H. Burke, *Advances in Physics: X* **7**, 1946426 (2022).
- [10] C. L. Degen, F. Reinhard, and P. Cappellaro, *Reviews of modern physics* **89**, 035002 (2017).
- [11] S. E. Crawford, R. A. Shugayev, H. P. Paudel, P. Lu, M. Syamlal, P. R. Ohodnicki, B. Chorpene, R. Gentry, and Y. Duan, *Advanced Quantum Technologies* **4**, 2100049 (2021).
- [12] Y. Wang, Z. Hu, and S. Kais, *Photonic Quantum Technologies: Science and Applications* **2**, 651 (2023).
- [13] N. Aslam, H. Zhou, E. K. Urbach, M. J. Turner, R. L. Walsworth, M. D. Lukin, and H. Park, *Nature Reviews Physics* **5**, 157 (2023).
- [14] R. Schnabel, N. Mavalvala, D. E. McClelland, and P. K. Lam, *Nature Comm.* **1**, 121 (2010).
- [15] L. Pezze, A. Smerzi, M. K. Oberthaler, R. Schmied, and P. Treutlein, *Rev. Mod. Phys.* **90**, 035005 (2018).
- [16] E. Polino, M. Valeri, N. Spagnolo, and F. Sciarrino, *AVS Quant. Sci.* **2** (2020).
- [17] G. Vidal, *J. Mod. Opt.* **47**, 355–376 (2000).
- [18] F. Verstraete, J. Dehaene, and B. De Moor, *Phys. Rev. A* **68** (2003), 10.1103/physreva.68.012103.

- [19] A. Osterloh and J. Siewert, *Phys. Rev. A* **72**, 012337 (2005).
- [20] D. Ž. Đoković and A. Osterloh, *J. Math. Phys.* **50**, 033509 (2009).
- [21] S. Hill and W. K. Wootters, *Phys. Rev. Lett.* **78**, 5022 (1997).
- [22] W. K. Wootters, *Phys. Rev. Lett.* **80**, 2245–2248 (1998).
- [23] V. Coffman, J. Kundu, and W. K. Wootters, *Phys. Rev. A* **61** (2000), 10.1103/physreva.61.052306.
- [24] L. Gurvits, in *Proceedings of the thirty-fifth annual ACM symposium on Theory of computing*, STOC03 (ACM, 2003) p. 10–19.
- [25] L. Gurvits, *J. Comp. Sys. Sci.* **69**, 448–484 (2004).
- [26] R. Y. Wen, G. Perez, W. Witzak-Krempa, and A. Kempf, [arXiv:2410.05400](https://arxiv.org/abs/2410.05400) (2024), 10.48550/ARXIV.2410.05400.
- [27] J. Neveling and A. Osterloh, [arXiv:2411.15032](https://arxiv.org/abs/2411.15032) (2024).
- [28] R. Lohmayer, A. Osterloh, J. Siewert, and A. Uhlmann, *Phys. Rev. Lett.* **97**, 260502 (2006).
- [29] C. Eltschka, A. Osterloh, J. Siewert, and A. Uhlmann, *New J. Phys.* **10**, 043014 (2008).
- [30] O. Viehmann, C. Eltschka, and J. Siewert, *Appl. Phys. B* **106**, 533 (2012).
- [31] A. Osterloh, *Phys. Rev. A* **94**, 062333 (2016).
- [32] C. Carathéodory, *Rendiconti Del Circolo Matematico di Palermo (1884-1940)* **32**, 193 (1911).
- [33] A. Uhlmann, *Open Syst. Inf. Dyn.* **5**, 209 (1998).
- [34] O. Viehmann, C. Eltschka, and J. Siewert, *Phys. Rev. A* **83** (2011), 10.1103/physreva.83.052330.